NASA TM X-57

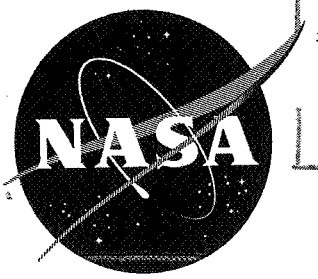

TECHNICAL MEMORANDUM
X - 57

FLIGHT INVESTIGATION OF LOADS ON A TEE-TAIL AT TRANSONIC AND SUPERSONIC SPEEDS

By William L. Marcy

High-Speed Flight Station
Edwards, Calif.

NATIONAL AERONAUTICS AND SPACE ADMINISTRATION

WASHINGTON

September 1959

NATIONAL AERONAUTICS AND SPACE ADMINISTRATION

TECHNICAL MEMORANDUM X-57

FLIGHT INVESTIGATION OF LOADS ON A TEE-TAIL AT TRANSONIC AND SUPERSONIC SPEEDS*

By William L. Marcy

SUMMARY

Flight-measured horizontal- and vertical-tail loads on a supersonic fighter airplane at Mach numbers from 0.81 to 2.06 and altitudes from 20,000 to 55,000 feet are compared with wind-tunnel data and theoretical results.

The variation with Mach number of the horizontal-tail lift-curve slope obtained from abrupt stabilizer pulses was influenced by altitude, an effect which was attributed to aeroelasticity. Adjusting the data to rigid-surface conditions increased the measured values of lift-curve slope by 5 to 20 percent. The horizontal-tail-panel spanwise center of load was essentially constant at about 45 percent of the panel span, with no aeroelastic effects noted.

Vertical-tail lift-curve slopes obtained during yawing oscillations showed no effects of angle of attack for the low angle-of-attack range tested. Adjusting the data to rigid-surface conditions increased the measured lift-curve slopes by 5 to 12 percent. The spanwise center of load of the vertical tail was at about 38 percent of the panel span for all speeds and altitudes.

The influence of sideslip on the horizontal tail was large, producing an unsymmetrical lift component per degree of sideslip that was almost as large as the horizontal-tail lift-curve slope in the low supersonic speed range. At subsonic and high supersonic speeds this interference effect reduced to about half the value of the corresponding symmetrical lift-curve slope. Horizontal-tail spanwise centers of load during yawing oscillations were at about 35 percent of the panel span over most of the speed range covered.

In most cases, excellent agreement was found between wind-tunnel results and flight results. Theoretical values of lift-curve slopes were

5 to 20 percent greater than experimental values, and theoretical values of spanwise center of load were in good agreement with the flight results. It was concluded that calculations of a preliminary-design type gave adequate predictions of forces and bending moments on tee-tails for small angles of attack and sideslip in the transonic and supersonic speed ranges.

INTRODUCTION

Accurate computation of horizontal- and vertical-tail effectiveness in airplane design is difficult because of the complex flow conditions at the tail. To verify or correct the design estimates, wind-tunnel tests of the specific configuration are therefore required. Since these tests do not always duplicate flight conditions, some comparison with flight data is considered desirable. Such a comparison is of particular interest with respect to the tee-tail, inasmuch as flight information on this configuration is relatively limited.

One of the principal advantages of the tee-tail configuration is an increase in tail effectiveness over that of conventional configurations. The effectiveness of the horizontal tail is increased by its elevation above the wing-fuselage wake and downwash, and the vertical-tail effectiveness is increased by the end-plate effect of the horizontal tail at its tip. Among the disadvantages of a tee-tail installation are reduced longitudinal stability at high angles of attack and susceptibility to complex flutter modes.

A supersonic fighter airplane with a tee-tail has been extensively tested by the NASA in wind tunnels and in flight. References 1 to 5 present results of some of the wind-tunnel tests. In this paper, results of flight measurements of horizontal- and vertical-tail loads are presented, showing the effects of angle of attack and sideslip at transonic and supersonic speeds. A discussion of some interference effects is included, and comparisons are made of flight results, wind-tunnel data, and theoretical calculations.

SYMBOLS

b panel span outboard of strain-gage station, ft

C_B bending-moment coefficient, $\frac{\text{Bending moment}}{qSb}$

C_N horizontal-tail normal-force coefficient, $\frac{\text{Normal force}}{qS_h}$

$C_{N_{\alpha_h}}$	slope of variation of horizontal-tail normal-force coefficient with horizontal-tail angle of attack
C_Y	vertical-tail side-force coefficient, $\frac{\text{Side force}}{qS_v}$
$C_{Y_{\beta_v}}$	slope of variation of vertical-tail side-force coefficient with sideslip angle
cp	spanwise center of load, percent panel span outboard of strain-gage station
g	acceleration due to gravity, ft/sec^2
h_p	pressure altitude, ft
i_h	horizontal-stabilizer deflection, deg
M	Mach number
q	dynamic pressure, lb/sq ft
S	panel area outboard of strain-gage station, sq ft
t	time, sec
α	airplane angle of attack, deg
β	airplane angle of sideslip, deg
δ_{yd}	yaw-damper deflection, deg

Subscripts:

h	horizontal-tail panel
L	left horizontal-tail panel
R	right horizontal-tail panel
v	vertical-tail panel
u	unsymmetrical

AIRPLANE

The test airplane is a single-place, jet-powered fighter airplane with a speed capability in excess of a Mach number of 2. The airplane has a thin, low-aspect-ratio wing, unswept at the 70-percent-chord line, and a tee-tail. The leading edge of the tapered vertical tail is swept 44°, and the aspect ratio is 0.849, based on the exposed area. The

all-movable horizontal tail is unswept at the midchord and has an aspect ratio of 2.95. The lateral and longitudinal controls are fully powered, with artificial feel provided for the pilot. The rudder, which is unpowered, is locked in neutral position at supersonic speeds. Automatic pitch, roll, and yaw dampers are incorporated, but were not in operation during the tests reported in this paper.

Table I presents pertinent physical characteristics of the airplane. A three-view drawing is shown in figure 1, and a photograph is presented in figure 2.

INSTRUMENTATION AND ACCURACY

The following quantities pertinent to this investigation were measured:

Airspeed
Altitude
Angle of attack and angle of sideslip
Control-surface positions
Normal, longitudinal, and lateral linear accelerations
Pitching, rolling, and yawing accelerations and velocities
Horizontal- and vertical-tail loads

All data were recorded on standard NASA internal-recording instruments. Film records were correlated by a common timer.

Loads were measured with bakelite strain-gage bridges installed at the right and left horizontal-tail roots and at the vertical-tail root. The bridge outputs were recorded on a 36-channel oscillograph.

The shears and bending moments presented in this paper are direct measurements of the aerodynamic loads, since inertia loads were negligible. The angles of attack and sideslip are measured values uncorrected for flow angularity, angular velocities, or interference effects. The estimated accuracies of the quantities used herein are:

M	±0.01 (±0.015 transonic)
i_h, deg	±0.1
α (incremental), deg	±0.1
β (incremental), deg	±0.1
Measured shear, lb	±100
Measured bending moment, in-lb	±1,000

TESTS

Flight tests were performed at the NASA High-Speed Flight Station at Edwards, Calif. The tests consisted of abrupt horizontal-tail pulses to obtain horizontal-tail loads and of abrupt deflections of the yaw-damper surface, which induced yawing oscillations, to obtain vertical-tail loads. Horizontal-tail pulses were made from 1g level flight; yawing maneuvers were made at normal accelerations of 0.5, 1.0, 1.5, and 2.0g. Nominal altitudes were 20,000, 40,000, and 55,000 feet, and the speed range covered was from a Mach number of 0.81 to 2.06. Reynolds numbers based on horizontal-tail mean aerodynamic chord varied from 5.7×10^6 to 22.5×10^6, depending on altitude and Mach number.

RESULTS AND DISCUSSION

Horizontal-Tail Loads

Presented in figure 3 are typical time histories of stabilizer deflection, angle of attack, and right and left horizontal-tail-panel normal-force coefficients and bending-moment coefficients during a stabilizer-pulse maneuver. Only the initial and maximum values of horizontal-tail deflection i_h and the corresponding horizontal-tail-panel normal-force and bending-moment coefficients C_N and C_B were utilized in the analysis. The ratio of incremental normal-force coefficient to incremental horizontal-stabilizer deflection is the normal-force-curve slope of the horizontal tail, since angle-of-attack changes during the initial portion of the control input were negligible. Because the angle of attack of the surface was small, the normal-force coefficient was approximately equal to the lift coefficient; these terms are used interchangeably in this paper. Effects of lag in the buildup of lift were considered but were also negligible, since only 0.03 second, at most, was required to reach 95 percent of steady-state lift, and the time to reach maximum horizontal-stabilizer deflection was about 0.15 second.

Figure 4(a) presents the variation of horizontal-tail-panel normal-force-curve slope $C_{N_{\alpha_h}}$ with Mach number, obtained from pulse data. The values of lift-curve slope shown are averages of right- and left-panel values for each maneuver, which generally differed less than 0.004 per degree. The flight results showed lift-curve slopes that were generally lower for the low-altitude maneuvers than for maneuvers at high altitudes. Aeroelastic corrections obtained from the manufacturer's design data were therefore used to transform the flight results to rigid

conditions; the adjusted data are shown in figure 4(b) for a rigid horizontal tail. These corrections increased the flight-determined values by 5 to 20 percent, depending on altitude and Mach number.

Also shown in figure 4(b) are results obtained from wind-tunnel tests and theoretical calculations. The wind-tunnel results were from the model buildup data of references 1 and 3. The subsonic data were reduced to horizontal-tail lift-curve slopes from values of incremental airplane pitching-moment coefficient due to horizontal-tail deflection, whereas the supersonic data were obtained from a faired line showing the variation with Mach number of the incremental airplane lift coefficient due to horizontal-tail deflection. The theoretical lift-curve slope was calculated for subsonic speeds by using the method of reference 6, and for supersonic speeds by using reference 7. These methods are for thin, isolated wings without twist or camber and are, therefore, calculations of the type that would be made for preliminary-design purposes.

As can be seen in figure 4(b), the agreement between wind-tunnel and flight results corrected for aeroelasticity is good at all speeds. Theoretical calculations at subsonic speeds indicate excellent agreement with experimental results. At supersonic speeds, the theoretical values are 5 to 20 percent higher than the experimental values. These differences are considered to result from the fact that the theoretical surface is a flat plate of zero thickness in a uniform stream, whereas the experimental surface has thickness, curved surfaces, and is subject to shock waves emanating from the wings and vertical tail.

The variation of horizontal-tail-panel spanwise center of load with Mach number is presented in figure 5. The spanwise center of load was obtained by taking the ratio of incremental horizontal-tail-panel bending moment to horizontal-tail-panel normal force for the pulse maneuvers. Theoretical values of the spanwise center of load for rigid conditions were obtained for supersonic speeds from charts presented in reference 8 and are shown as the solid line in figure 5. The experimental spanwise center of load is seen to be about 5-percent panel span outboard of the theoretical value, which is essentially constant at all supersonic speeds. Because of the scatter in the data of figure 5, aeroelastic effects could not be seen; hence, calculations of these effects were not made.

Vertical-Tail Loads

Inasmuch as the rudder is locked at supersonic speeds and was also locked for the subsonic directional maneuvers reported in this paper, variations of sideslip angle were obtained by momentarily operating the yaw-damper control to maximum deflection, then returning it to zero; a small oscillation in sideslip is thus induced. A typical time history of such a maneuver is shown in figure 6, which presents the variations

with time of yaw-damper deflection δ_{yd}, sideslip angle β, vertical-tail-panel side-force and bending-moment coefficients C_{Y_v} and C_{B_v}, and horizontal-tail-panel normal-force and bending-moment coefficients C_N and C_B. Yawing oscillations were obtained at altitudes of 20,000, 40,000, and 55,000 feet and at angles of attack from 1° to 5°, corresponding to normal accelerations of 0.5 to 2.0g.

It is noted that the area of the yaw-damper control is so small that the change in C_{Y_v} with yaw-damper deflection is not detected. A second point to be noted in this figure is that the sideslip angle oscillates about an indicated angle of 0.5°. This indication of a trim sideslip angle other than zero is due mainly to interference from the angle-of-attack vane on the sideslip vane at supersonic speeds. Since the Mach number was constant during each maneuver and the oscillations were small, the interference error is a constant and the incremental accuracy of sideslip measurement is within $\pm 0.1^\circ$, although the absolute angle may be a degree or more in error.

Shown in figure 7 are the variations of vertical-tail-panel lift-curve slope with Mach number for flight, wind-tunnel, and theoretical calculations. The flight-determined values were obtained by plotting the variations of vertical-tail-panel side-force coefficient with sideslip angle during yawing oscillations, and determining the slopes. Aeroelastic corrections were then applied, using the airplane manufacturer's design data, to obtain rigid-surface values. These corrections increased the basic lift-curve slope by 5 to 12 percent, depending on speed and altitude. The flight data do not show any discernible influences of angle of attack or altitude over the angle-of-attack range of 1° to 5° for which data are shown.

Wind-tunnel-model buildup data from references 2, 4, and 5 were used to obtain the vertical-tail contribution to the variation of airplane side-force coefficient C_Y with sideslip and were converted to vertical-tail-panel lift-curve slope. To account for interference effects between the fuselage and the vertical tail in making the conversion from airplane coefficients based on wing area to vertical-tail coefficients, the area of the vertical tail projected to the fuselage center line was used. The scatter in the wind-tunnel data is probably due to the difficulty in obtaining slopes from small plots and in subtracting numbers with small differences.

Theoretical calculations of the vertical-tail-panel lift-curve slope were made by using the charts of reference 6 for subsonic speeds and reference 9 for supersonic speeds. As discussed in the Horizontal-Tail Loads section, these calculations are of a preliminary-design type. By using the results presented in reference 10, the horizontal tail was

estimated to increase the vertical-tail geometric aspect ratio from 0.849 to an effective aspect ratio of 1.13, an increase of 33 percent, because of the end-plate effect. The tail-alone lift-curve slope was then calculated, based on the effective aspect ratio, and the values were increased by 10 percent to account for fuselage effect. This 10-percent increase was based on an estimate that the fuselage was about half as effective as an infinite end plate. It is shown in reference 11 that an infinite end plate increases the lift-curve slope of a vertical tail about 20 percent at supersonic speeds.

It can be seen in figure 7 that the wind-tunnel and flight data are in excellent agreement except near $M = 1$, where the flight results are about 15 percent lower than wind-tunnel values, and at $M = 1.6$ where the wind-tunnel value is considerably lower. The theoretical calculations are in good agreement with both wind-tunnel and flight results, indicating that the relatively unsophisticated methods used are adequate for prediction of loads for the small angles of attack and sideslip considered.

It is shown in reference 12 that sidewash at supersonic speeds is generally low. No estimate of sidewash at subsonic speeds was made.

The variation of flight-determined vertical-tail-panel spanwise center of load cp_v with Mach number is presented in figure 8, together with comparable results of theoretical calculations. The flight-determined spanwise center of load was obtained by plotting the variation of vertical-tail-panel root bending-moment coefficient with vertical-tail-panel side-force coefficient for the yawing maneuvers, and obtaining the slope. Since the horizontal tail is above the vertical-tail root, unsymmetrical bending of the horizontal tail results in bending of the vertical tail. The measured vertical-tail bending moments were therefore corrected for the influence of unsymmetrical horizontal-tail loads by subtracting the difference between left and right horizontal-tail-panel bending moments from the vertical-tail root bending moment. The horizontal-tail-panel bending moments were first transferred 10 inches from the strain-gage station to the horizontal-tail center line to obtain the bending moment at the junction of the horizontal tail and the vertical tail. The vertical-tail root bending moment due to unsymmetrical horizontal-tail loads was generally about 50 percent of the total measured vertical-tail root bending moment. Although the data show considerable scatter, it appears that the vertical-tail-panel spanwise center of load is fairly constant at all speeds and altitudes for which data were obtained.

The theoretical value of the vertical-tail-panel spanwise center of load was obtained by assuming that the strong end-plate effects of the fuselage and vertical tail result in nearly two-dimensional flow. The spanwise load distribution is therefore plan form in shape, and the

center of load is at 42-percent panel span, which is about 4-percent panel span farther outboard than the average of the experimental data.

Interference Effects

Effects of vertical tail on horizontal tail.- Unsymmetrical pressures on the vertical tail during yawing oscillations are transmitted to the horizontal tail and result in unsymmetrical horizontal-tail loads. Because the total horizontal-tail load was constant, the increase in load on one panel is accompanied by a corresponding decrease on the opposite panel. The variation of unsymmetrical horizontal-tail load per panel with sideslip was plotted for the yawing maneuvers summarized in figures 7 and 8. The slopes of these plots are presented in figure 9 as the variation of $\frac{dC_{N_u}}{d\beta}$ with Mach number. Also presented in this figure for comparison are the symmetrical lift-curve slopes shown in figure 4(b).

It can be seen that the increment of unsymmetrical load per degree of sideslip is relatively small compared to the symmetrical lift-curve slope at subsonic speeds, whereas at low supersonic speeds this increment is nearly as great as the symmetrical lift-curve slope. At higher supersonic speeds the effect of sideslip decreases rapidly, both because of the usual reduction of lift at supersonic speeds and because more of the horizontal-tail area extends ahead of the Mach lines from the vertical tail as speed is increased and is, therefore, unaffected by interference from the vertical tail. Effects of altitude are not apparent in these data, indicating that aeroelastic effects on the unsymmetrical loads were small.

Shown in figure 10 are the variations of spanwise center of load with Mach number for the right and left horizontal-tail panels during yawing oscillations. These data were obtained by taking the slopes of horizontal-tail-panel bending-moment coefficient plotted against horizontal-tail normal-force coefficient. The data are widely scattered about an average of 35 to 38 percent of the panel span. For comparison, the centers of load for longitudinal pulses (symmetrical loads) shown in figure 5 are also presented in figure 10. It can be seen that the spanwise center of load in yawing maneuvers is inboard of the center of load for symmetrical loads. This is a reasonable result, since pressure distributions at inboard stations would be expected to be affected more by vertical-tail interference than those at outboard stations; thus, the bending moments due to interference effects would be less than for symmetrical loads. Although the difference between the centers of pressure on the right and left horizontal-tail panels was usually 3 to 10 percent, no consistent trend was noted, and the values presented in figure 10 are therefore the average of right and left values. The variation of bending moment with shear was linear as each panel oscillated from positive to

negative sideslip, indicating no difference between upwind and downwind centers of pressure. No effects of altitude or aeroelasticity were noted.

Effects of horizontal tail on vertical tail.- The principal interference effect on the vertical tail is, of course, the increase in lift-curve slope resulting from the addition of the horizontal tail. Although flight data on this effect cannot be obtained, theoretical calculations showed that the estimated 36-percent increase in vertical-tail aspect ratio resulted in about a 10-percent increase in the lift-curve slope of the vertical tail. These calculations agreed with the wind-tunnel results at subsonic speeds, but at supersonic speeds the wind-tunnel data showed little or no increase in the vertical-tail-panel side-force coefficient when the horizontal tail was added.

CONCLUSIONS

Flight measurements of horizontal- and vertical-tail loads on a supersonic fighter airplane at Mach numbers from 0.81 to 2.06 and altitudes from 20,000 to 55,000 feet were compared with wind-tunnel data and results of theoretical calculations with the following results:

1. The variation with Mach number of the horizontal-tail lift-curve slope obtained from abrupt stabilizer pulses was influenced by altitude, an effect which was attributed to aeroelasticity. Adjusting the data to rigid-surface conditions increased the measured values of lift-curve slope by 5 to 20 percent, depending on the dynamic pressure and Mach number. The horizontal-tail-panel spanwise center of load was essentially constant at about 45 percent of the panel span, with no aeroelastic effects noted.

2. Lift-curve slopes of the vertical tail obtained from yawing oscillations showed no effects of angle of attack for the angle-of-attack range of 1° to 5° tested. Adjusting to rigid-surface conditions increased the measured lift-curve slopes by 5 to 12 percent. The spanwise center of load of the vertical tail was at about 38-percent panel span for all speeds and altitudes.

3. The influence of sideslip on the horizontal tail was large, producing an unsymmetrical lift component per degree of sideslip that was almost as large as the lift-curve slope of the horizontal tail in the low supersonic speed range. At subsonic and high supersonic speeds this interference effect was about half of the corresponding symmetrical lift-curve slope. Spanwise centers of load measured on the horizontal tail during yawing oscillations were about 35 percent of the panel span over most of the speed range covered.

4. Excellent agreement was found in most cases between wind-tunnel results and flight results. Theoretical values of lift-curve slopes were 5 to 20 percent greater than experimental values, and theoretical values of spanwise center of load were in good agreement with the flight results. It was concluded that calculations of a preliminary-design type gave adequate predictions of forces and bending moments on tee-tails for small angles of attack and sideslip through the transonic and supersonic speed ranges.

High-Speed Flight Station,
National Aeronautics and Space Administration,
Edwards, Calif., May 19, 1959.

REFERENCES

1. Smith, Willard G.: Wind-Tunnel Investigation at Subsonic and Supersonic Speeds of a Fighter Model Employing a Low-Aspect-Ratio Unswept Wing and a Horizontal Tail Mounted Well Above the Wing Plane. Longitudinal Stability and Control. NACA RM A54D05, 1954.

2. Wetzel, Benton E.: Wind-Tunnel Investigation at Subsonic and Supersonic Speeds of a Fighter Model Employing a Low-Aspect-Ratio Unswept Wing and a Horizontal Tail Mounted Well Above the Wing Plane. Lateral and Directional Stability. NACA RM A54H26b, 1955.

3. Hieser, Gerald, and Reid, Charles F., Jr.: Transonic Longitudinal Aerodynamic Characteristics of a Fighter-Type Airplane Model With a Low-Aspect-Ratio Unswept Wing and a Tee-Tail. NACA RM L54K19a, 1956.

4. Arabian, Donald D., and Schmeer, James W.: Lateral Stability and Control Measurements of a Fighter-Type Airplane With a Low-Aspect-Ratio Unswept Wing and a Tee-Tail. NACA RM L55F08, 1956.

5. Holtzclaw, Ralph W.: Wind-Tunnel Investigation of Devices to Improve Static Directional Stability of an Unswept-Wing Airplane Model at Mach Numbers From 0.8 to 2.2. NASA MEMO 10-4-58A, 1958.

6. DeYoung, John, and Harper, Charles W.: Theoretical Symmetric Span Loading at Subsonic Speeds for Wings Having Arbitrary Plan Form. NACA Rep. 921, 1948.

7. Martin, John C., Margolis, Kenneth, and Jeffreys, Isabella: Calculation of Lift and Pitching Moments Due to Angle of Attack and Steady Pitching Velocity at Supersonic Speeds for Thin Sweptback Tapered Wings With Streamwise Tips and Supersonic Leading and Trailing Edges. NACA TN 2699, 1952.

8. Martin, John C., and Jeffreys, Isabella: Span Load Distributions Resulting From Angle of Attack, Rolling, and Pitching for Tapered Sweptback Wings With Streamwise Tips. Supersonic Leading and Trailing Edges. NACA TN 2643, 1952.

9. Harmon, Sidney M., and Jeffreys, Isabella: Theoretical Lift and Damping in Roll of Thin Wings With Arbitrary Sweep and Taper at Supersonic Speeds. Supersonic Leading and Trailing Edges. NACA TN 2114, 1950.

10. Riley, Donald R.: Effect of Horizontal-Tail Span and Vertical Location on the Aerodynamic Characteristics of an Unswept Tail Assembly in Sideslip. NACA Rep. 1171, 1954.

11. Martin, John C., and Malvestuto, Frank S., Jr.: Theoretical Force and Moments Due to Sideslip of a Number of Vertical Tail Configurations at Supersonic Speeds. NACA TN 2412, 1951.

12. Spearmen, M. Leroy: Some Factors Affecting the Static Longitudinal and Directional Stability Characteristics of Supersonic Aircraft Configurations. NACA RM L57E24a, 1957.

[redacted]

TABLE I.- PHYSICAL CHARACTERISTICS OF THE TEST AIRPLANE

Airplane:	
Length, overall, ft	54.7
Normal center-of-gravity location, percent wing mean aerodynamic chord	5.0
Wing span, ft	21.9
Wing area, sq ft	196.1
Mean aerodynamic chord, ft	9.56
Aspect ratio	2.45
Taper ratio	0.378
Leading-edge-sweep angle, deg	27.3
Airfoil thickness, percent chord	3.36
Horizontal tail:	
Span, ft	11.9
Area, sq ft	48.2
Mean aerodynamic chord, ft	4.42
Aspect ratio	2.95
Taper ratio	0.311
Leading-edge-sweep angle, deg	19.6
Airfoil thickness, percent chord -	
Root	4.93
Tip	2.61
Strain-gage station, outboard of root, in.	10.0
Tail length, wing mean aerodynamic quarter chord to horizontal-tail mean aerodynamic quarter chord, ft	18.7
Height above vertical-tail root station, ft	4.67
Panel, each -	
Span, ft	5.12
Area, sq ft	19.19
Mean aerodynamic chord, ft	4.04
Aspect ratio	1.37
Taper ratio	0.344
Vertical tail:	
Span, ft	5.46
Area, sq ft	35.1
Mean aerodynamic chord, ft	6.88
Aspect ratio	0.849
Taper ratio	0.371
Leading-edge-sweep angle, deg	44.0
Airfoil thickness, percent chord -	
Root	4.25
Tip	5.00
Strain-gage station, above root, in.	5.0
Tail length, wing mean aerodynamic quarter chord to vertical-tail mean aerodynamic quarter chord, ft	15.14
Area projected to fuselage center line, sq ft	55.8
Yaw damper -	
Area, sq ft	1.0
Chord, ft	1.0
Span, ft	1.0
Panel -	
Span, ft	5.06
Area, sq ft	31.15
Mean aerodynamic chord, ft	6.60
Aspect ratio	0.827
Taper ratio	0.383

[redacted]

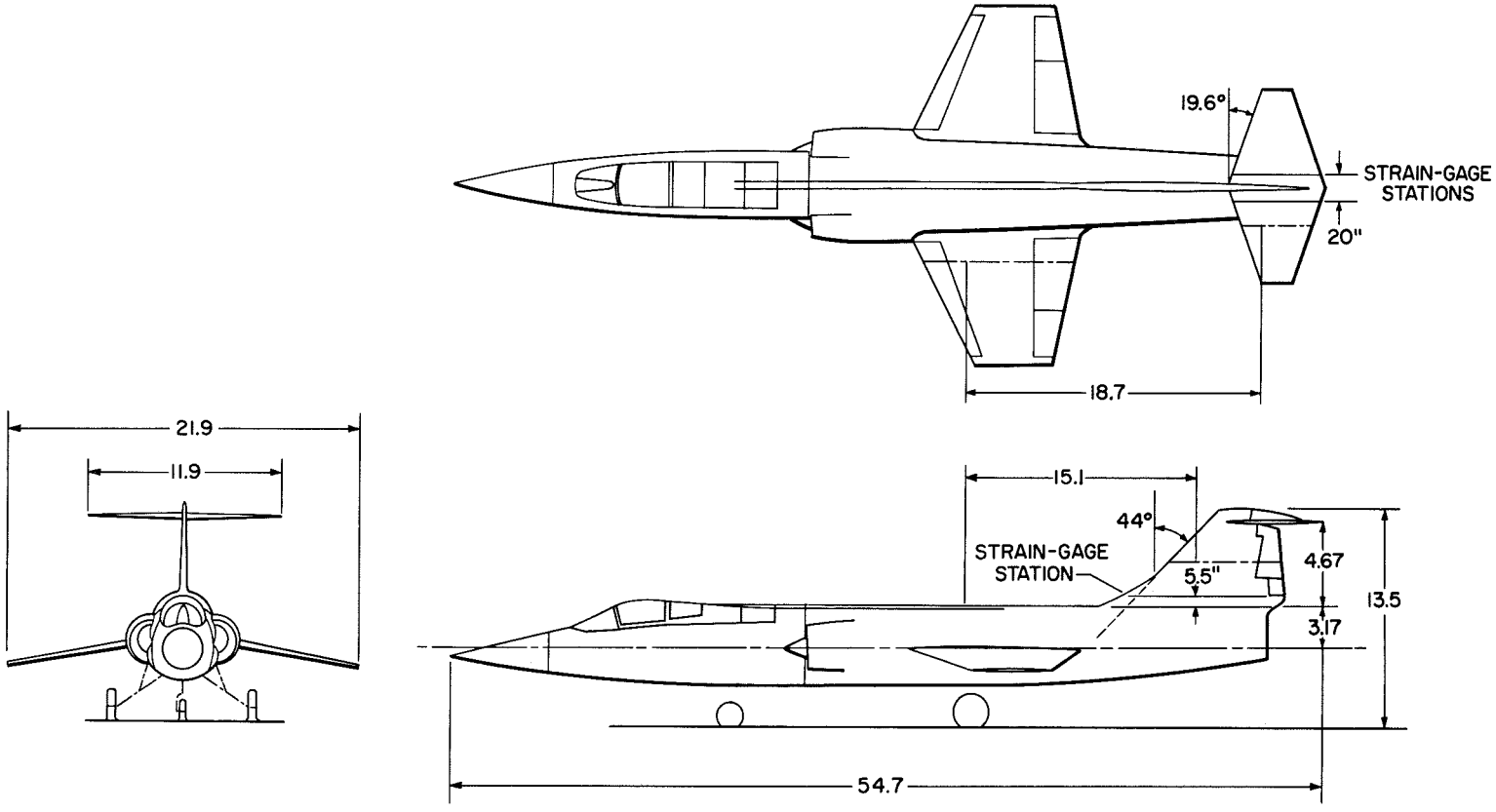

Figure 1.- Three-view drawing of the test airplane. All dimensions in feet except as noted.

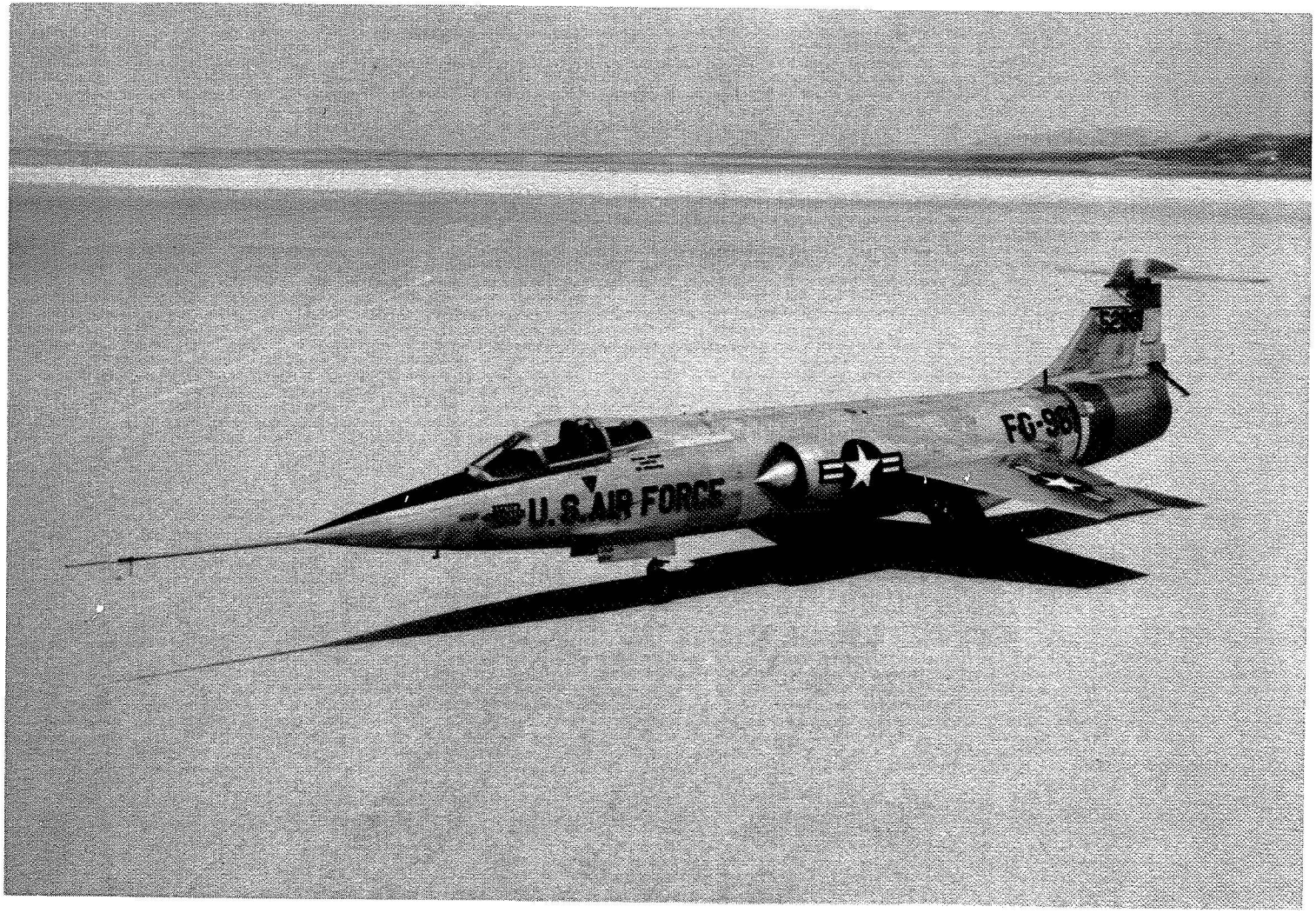

Figure 2.- Photograph of the test airplane. E-3022

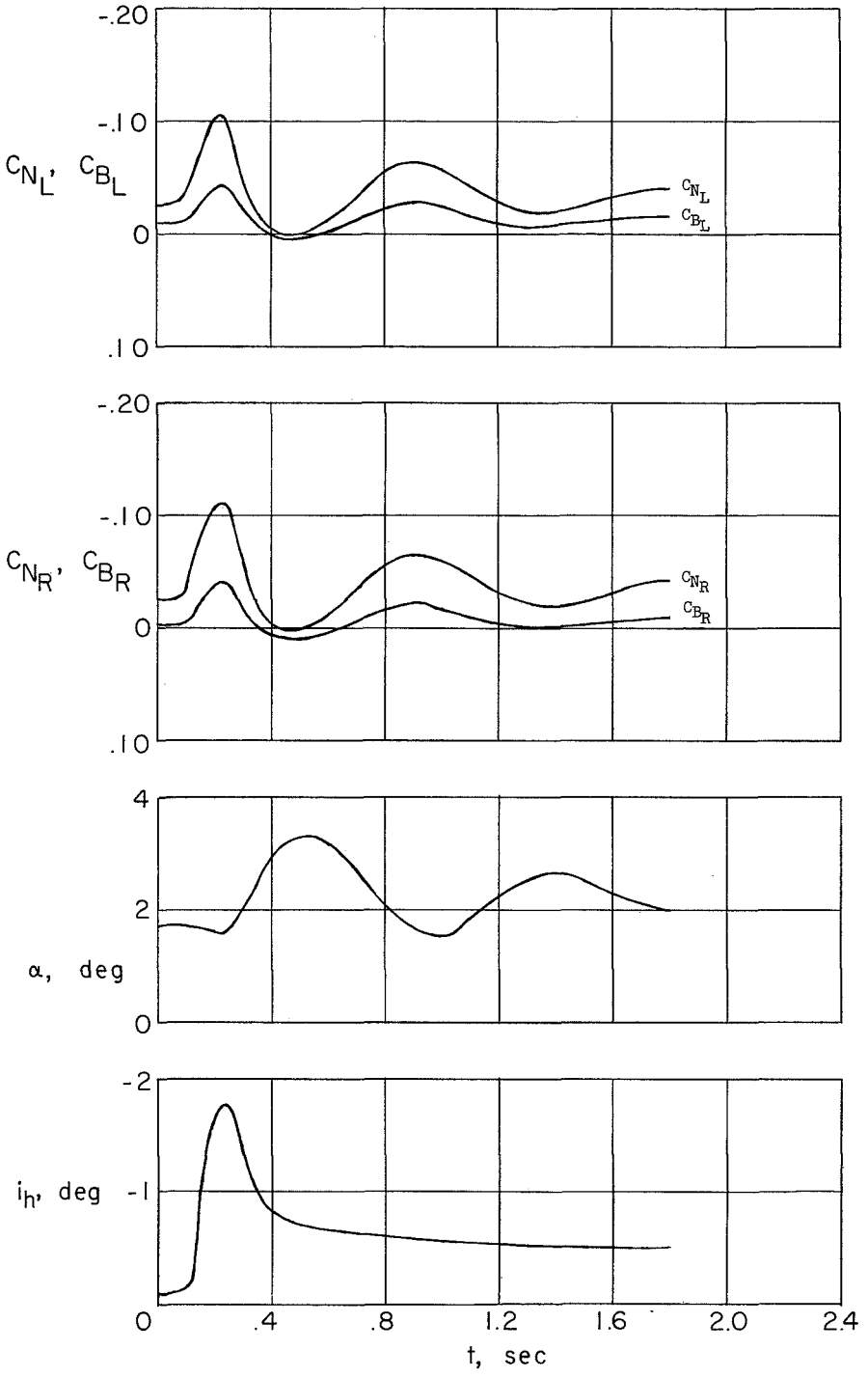

Figure 3.- Time history of a typical abrupt horizontal-tail pulse. M = 1.21; h_p = 20,000 feet.

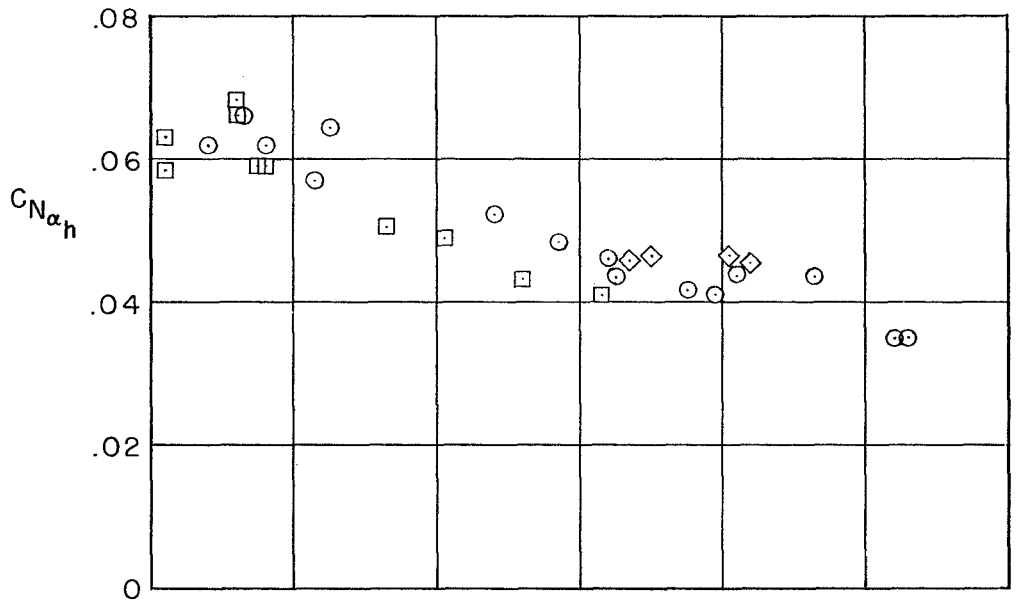

(a) Including aeroelastic effects.

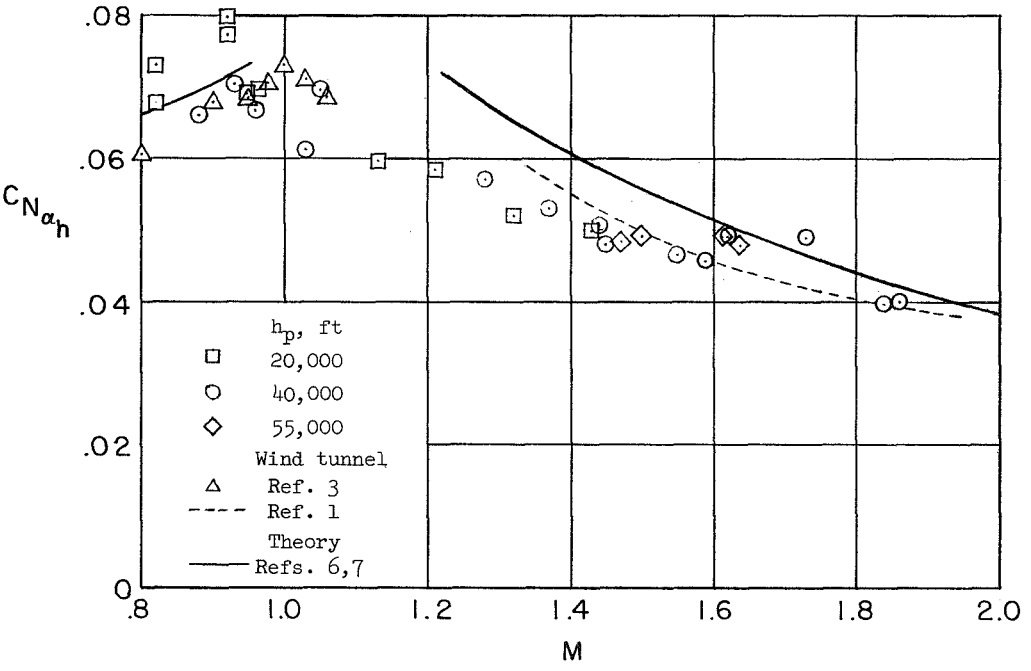

(b) Corrected to rigid horizontal-tail conditions.

Figure 4.- Variation of horizontal-tail-panel lift-curve slope with Mach number.

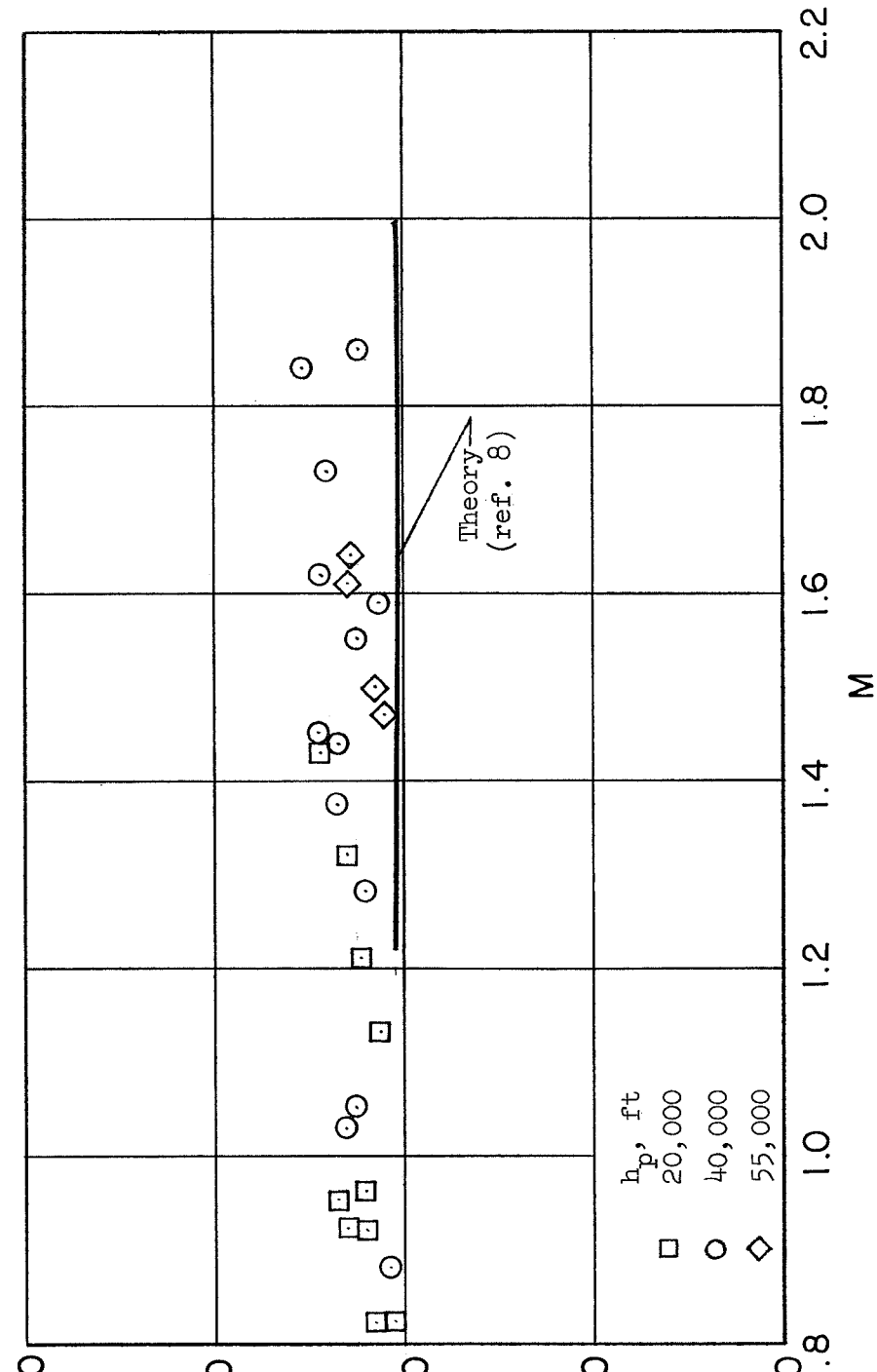

Figure 5.- Variation with Mach number of horizontal-tail-panel spanwise center of load during abrupt horizontal-tail pulses.

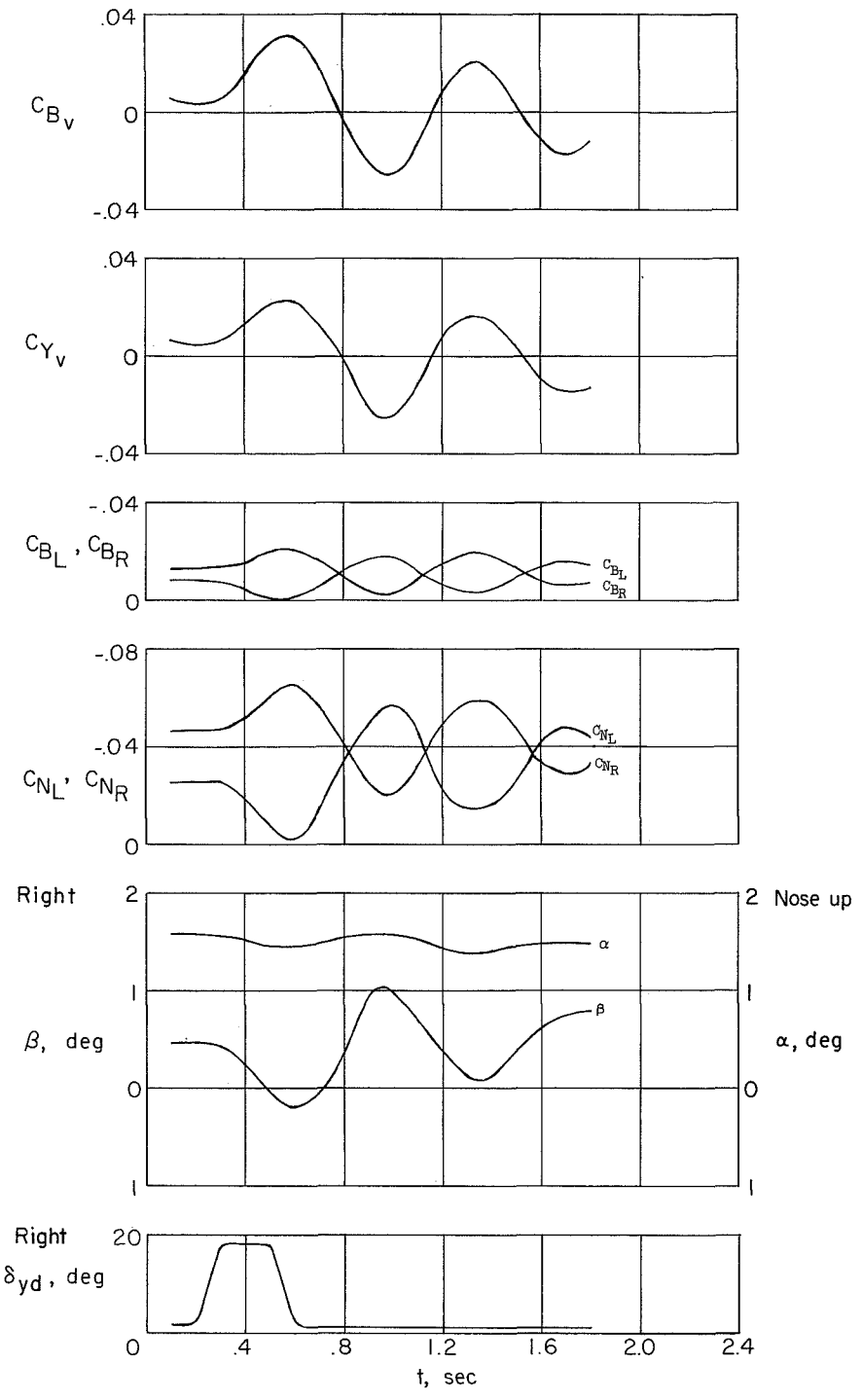

Figure 6.- Typical time history of an abrupt yaw-damper pulse. M = 1.22; h_p = 20,000 feet.

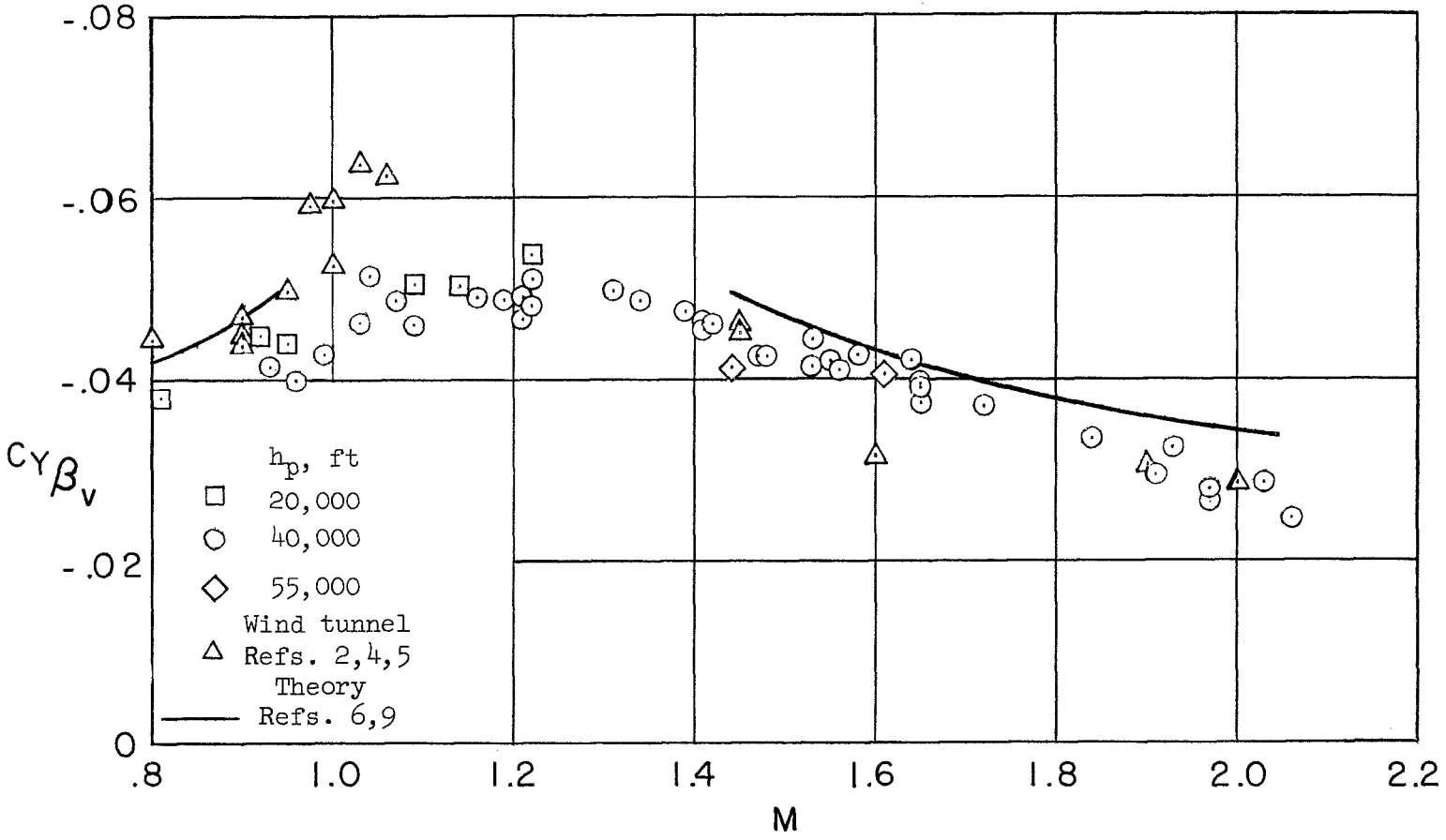

Figure 7.- Variation with Mach number of vertical-tail-panel lift-curve slope corrected to rigid-surface conditions.

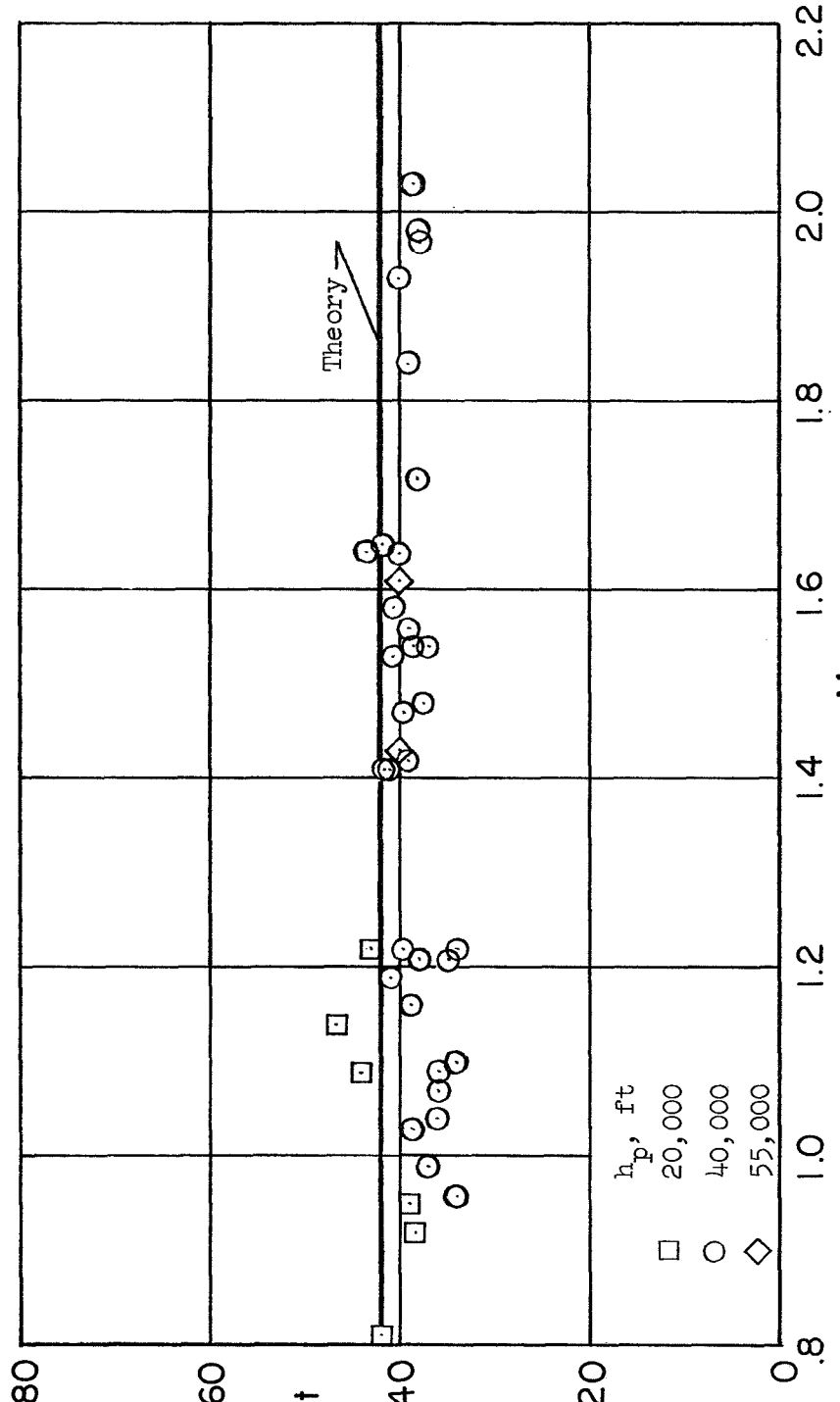

Figure 8.- Variation of vertical-tail-panel spanwise center of load with Mach number.

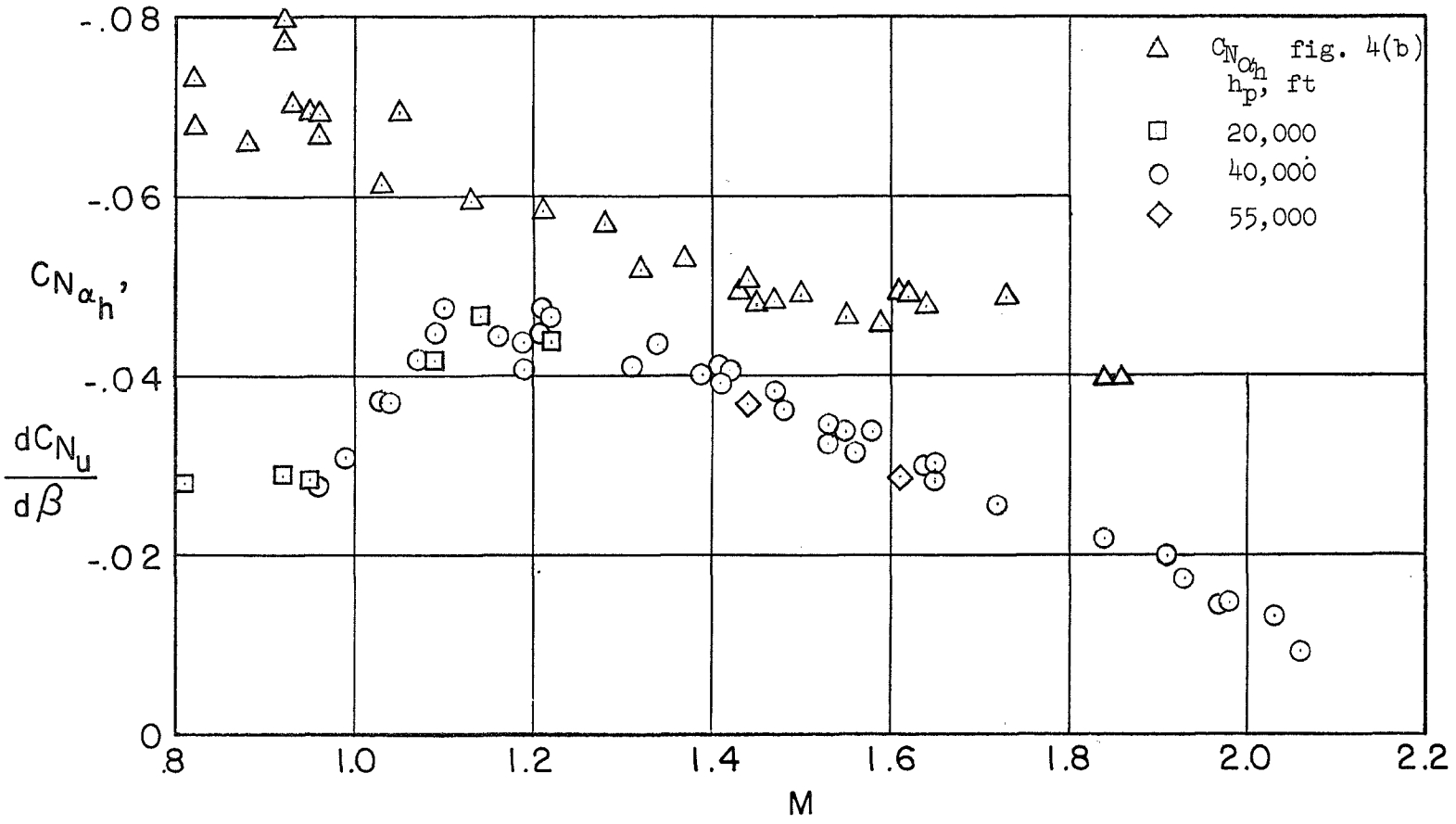

Figure 9.- Variation with Mach number of effect of sideslip on unsymmetrical horizontal-tail-panel normal-force coefficient.

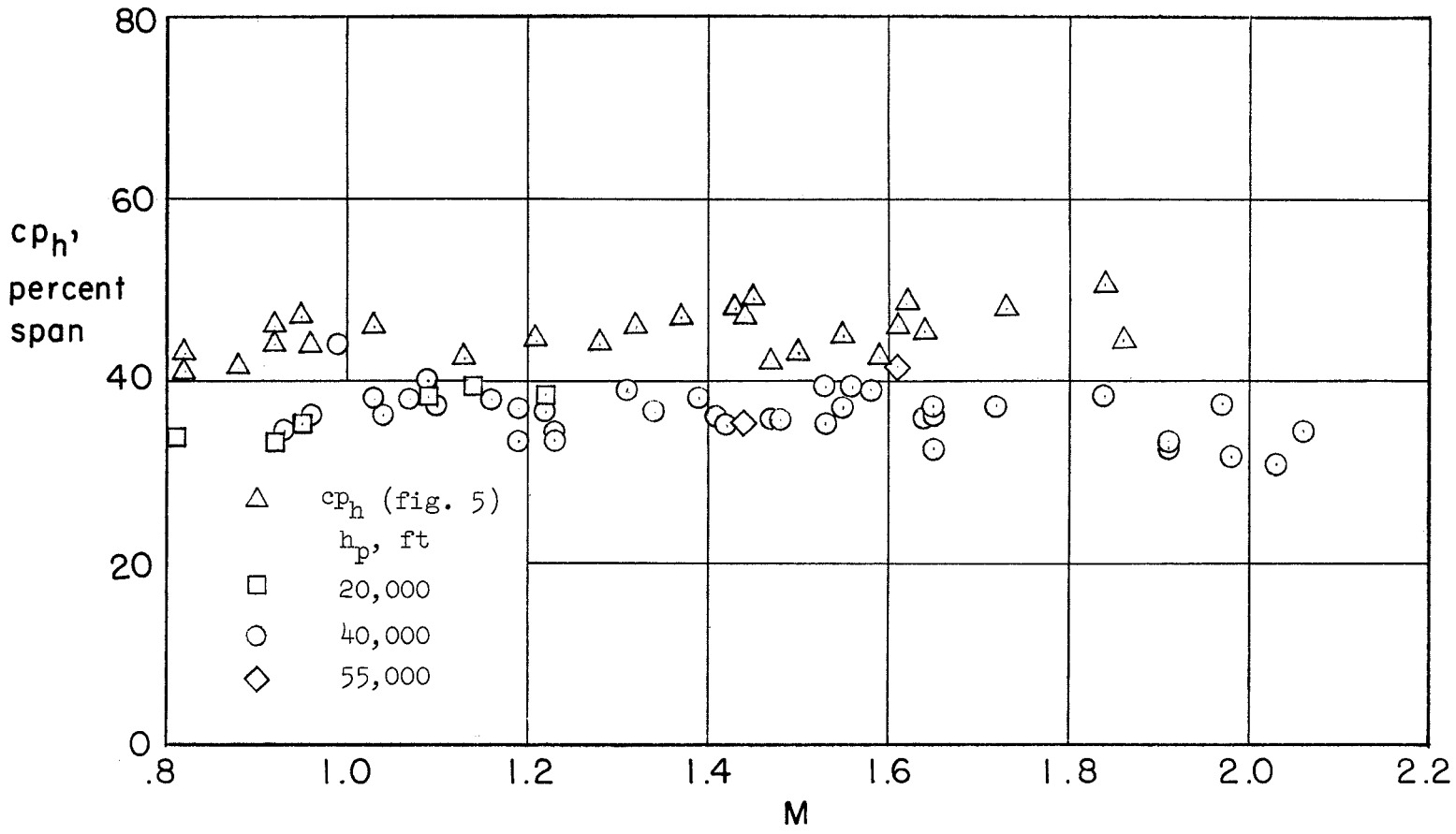

Figure 10.- Variation with Mach number of horizontal-tail-panel spanwise center of load during yawing oscillations.